GFD in Dedalus

A collection of simulations

Edited by

Ryan Shìjié Dù
Courant Institute of Mathematical Sciences - New York University

August 18, 2023

Contents

Chapter 1

Introduction

Ryan Shìjié Dù

This is a collection of computer simulations of Geophysical Fluid Dynamics (GFD) models using the Dedalus version 3 solver[1]. The combination of two delineates the content of this collection, which we will detail in this introduction. The editor's personal philosophy for modeling and simulation is also sprinkled throughout.

1.1 Dedalus

We will be using the newest version of the Dedalus solver, a flexible and efficient spectral partial differential equations solver. Dedalus comes with great documentation and a few illuminating examples that shows how to use it. This collection aims to expand on the list of examples by implementing models in GFD. Along the way we will introduce some tools and tricks that makes working with Dedalus easier, a list of them is in Section 1.1.2. These implementations could be the start of deeper study of these models, or they could be examples on how to use Dedalus.

1.1.1 Working with distributed parallelism via MPI

In particular, Dedalus uses distributed parallelism via MPI. Dedalus hides much of the complexity of working with MPI. However, an advanced user of Dedalus cannot forget its parallel architecture. All our examples work with multiple cores in distributed systems (a server with multiple nodes). For a tutoruial on how to use Dedalus v3 on the NYU Greene supercomputer, see this page: https://github.com/CAOS-NYU/Dedalusv3_GreeneSingularity.

1.1.2 Dedalus GFD tools

Adaptive timestep for when velocity is not a vector field The examples on Dedalus' website that have adaptive timestep uses the `d3.CFL` function, that take a vector field velocity as the input for calculating the timestep. However, often in GFD models, velocity comes from the derivatives of a streamfunction, and is not a vector field in Dedalus. We implement a simple CFL

[1] https://dedalus-project.org/

based adaptive timestep that take in the velocity as separate scalar fields. See the 2D Euler in Chapter ?? example for full details[2]. Note that we need to use the `d3.GlobalFlowProperty` to take maximum over MPI.

Calculating spectrum https://github.com/Empyreal092/GFD_in_Dedalus/blob/main/dedalus_subroutines/isospectrum.py

1.1.3 Desired features in Dedalus

Despite the power of Dedalus, there are some features we would like that is not currently implemented. This is a list of wants we have for Dedalus. We feel these should be possible to implement in the spectral set-up of Dedalus. We would be happy to contribute and implement them, but we are currently unclear how.

Arbitrary linear operators in doubly periodic domain We would like a way to define new linear operators that is only expressible as operations on the Fourier coefficient. More specifically, the linear operator $\mathcal{P}$ is defined by a user provided a matrix $\boldsymbol{P}$ such that

$$\mathcal{F}\{\mathcal{P}(\psi)\}_{\boldsymbol{k}} = \boldsymbol{P}_{\boldsymbol{k}}\hat{\psi}_{\boldsymbol{k}}. \tag{1.1}$$

where $\mathcal{F}$ and $\hat{\cdot}$ both means the Fourier transform and $\boldsymbol{P}_{\boldsymbol{k}}$ is the $\boldsymbol{k} = (k, \ell)$ element of the $\boldsymbol{P}$ matrix.

These operators are very common in GFD models. They include fractional and negative Laplacian of the form $|k|^{-d}$ used for the inversion in the famous α-turbulence models (Pierrehumbert, Held, and Swanson 1994; K. S. Smith et al. 2002) and for hypo-diffusion in turbulence simulation with inverse cascade (Callies et al. 2016; Majda, Mclaughlin, and Tabak 1997; Vallgren and Lindborg 2011). There are also more unconventional operators in the literature, e.g., the $\mathcal{P}$ in Xie 2020, (3.2):

$$\mathcal{P} = \frac{i}{2}\frac{\nabla^2}{-1 + \nabla^2/4} \tag{1.2}$$

where we have suppressed the geophysical constants for clarity. This operator still follows the form (1.2).

Going a bridge further, some linear operator takes vector Fourier coefficient. That is

$$\mathcal{F}\{\mathcal{P}(\boldsymbol{\psi})\}_{\boldsymbol{k}} = \boldsymbol{P}_{\boldsymbol{k}}\hat{\boldsymbol{\psi}}_{\boldsymbol{k}} \tag{1.3}$$

where

$$\boldsymbol{\psi}(x, y) = \begin{bmatrix} \psi_1(x, y) \\ \psi_2(x, y) \\ \vdots \\ \psi_n(x, y) \end{bmatrix} \tag{1.4}$$

is a n-vector of 2D fields and each $\boldsymbol{P}_{\boldsymbol{k}}$ is a n-by-n matrix. This means $\boldsymbol{P}$ is a $n \times n \times m \times m$ tensor where m is the maximally resolved wave numbers. An example of this kind of linear operator is

[2] https://github.com/Empyreal092/GFD_in_Dedalus/blob/main/2D_Euler/code/2D_Euler.py

Callies et al. 2016, which is a generalization of the Eady model (Eady 1949; Tulloch and K. Shafer Smith 2009). These operators essentially comes from Green's function of elliptic equations and reduce a 3D elliptic solve to a few 2D Fourier transforms. Being able to define these linear operators in Dedalus would be immensely helpful.

1.1.4 Shortcomings of Dedalus

Dedalus is not without its shortcomings. Here we list a few that we face occasionally. Compare with the last section, these are inherent deficiencies of the spectral method or needs significant software engineering to fix. We list them here to inform potential users know the sacrifice that comes with using Dedalus. But obviously we still love Dedalus as a tool since we are writing this collection.

Limited domain Being a spectral solver, Dedalus cannot solve problems that are on arbitrary domains.

A surprising discovery for us is that Dedalus cannot use parallelism on a closed box. In Cartesian settings, it needs a direction to be Fourier to be able to run in parallel[3]. This is disappointing since this exclude efficient simulation of classic models like the barotropic vorticity model of wind-driven gyres (Vallis 2017, §19.4).

1.2 Choice of models

In research, one comes up with the model first and choose the appropriate solver. Dedalus aims to be a component solve for many models. Since this collection is GFD in Dedalus, we take the opposite approach and pick models that is well set-up for Dedalus to solve. This means we will solve problems that are in periodic domain or on a circle or sphere. We aim to implement all GFD models that are commonly solve spectrally. This includes the examples in pyqg (https://pyqg.readthedocs.io/en/latest/equations.html) and GeophysicalFlows.jl(https://fourierflows.github.io/GeophysicalFlowsDocumentation/stable/). About SQG, see 1.1.3.

More importantly, Dedalus is a PDE solver. It is well suited to perform Direct Numerical Simulation (DNS), as opposed to Large Eddy Simulation (LES) or General Circulation Model (GCM). They are different tools that solve different problems. Dedalus is efficient enough for high enough resolution simulation that we assume all relevant dynamics of the model can be represented. We will use Dedalus to solve austere models in idealized set-ups. We take a philosophical approach well summarized in Vallis 2016:

> The moniker 'GFD' has also come to imply a methodology in which one makes the maximum possible simplifications to a problem, perhaps a seemingly very complex problem, seeking to reduce it to some bare essence. It suggests an austere approach, devoid of extraneous detail or superfluous description, so providing the fundamental principles and language for understanding geophysical flows without being overwhelmed by any inessentials that may surround the core problem. In this sense, GFD describes a method as well as an object of study.

[3] https://groups.google.com/u/1/g/dedalus-users/c/DVB995tMs-g/m/lSHGTZbBBgAJ

1.2.1 Nondimensionalization

One consequence of simulating austere models is that nondimensionalizing the equations often will produce only a few relevant nondimensional parameters for the dynamics. For us, this greatly simplifies the task of understanding the model and generalize the conclusion we obtain. We will always simulate the nondimensional version of the equations in the following examples. This agree with the approach of GeophysicalFlows.jl but contrast with that of pyqg[4].

In particular, we will use the notation of Vallis 1996:

> Here, and in the rest of the paper, expressions are written in dimensional form. The relevant non-dimensional parameters are also given, enclosed in curly brackets, {}. The pure dimensional form may be recovered simply by setting to unity the contents of the curly brackets. The non-dimensional form is recovered by setting all the physical parameters (such as g and f) to unity. This notation enables both the asymptotic ordering and physical appreciation of the terms to be facilitated.

For example, the Boussinesq system under the geostrophic scaling reads (cf. Vallis 2017, (PE.1-4)):

$$\{\mathrm{Ro}\}\left(\frac{\mathrm{D}u}{\mathrm{D}t} - \beta y v\right) - fv = -\phi_x, \tag{1.5}$$

$$\{\mathrm{Ro}\}\left(\frac{\mathrm{D}v}{\mathrm{D}t} + \beta y u\right) + fu = -\phi_y, \tag{1.6}$$

$$\phi_z = b, \tag{1.7}$$

$$\{\mathrm{Ro}\}\left(\frac{\mathrm{D}b}{\mathrm{D}t}\right) + \left\{\frac{\mathrm{Ro}^2}{\mathrm{Fr}^2}\right\} N^2 w = 0, \tag{1.8}$$

$$u_x + v_y + w_z = 0 \tag{1.9}$$

where we have the two nondimensional number

$$\{\mathrm{Ro}\} = \frac{U}{fL}; \qquad \{\mathrm{Fr}\} = \frac{U}{NH}. \tag{1.10}$$

[4]The examples use dimensional numbers, see https://pyqg.readthedocs.io/en/latest/examples/layered.html.

Chapter 2

Barotropic vorticity model

Ryan Shìjié Dù

We start with perhaps the most simple model of geophysical turbulence, barotropic vorticity model. We can write the model in vorticity form (ibid., §4.2.1):

$$\frac{\mathrm{D}}{\mathrm{D}t}\left(\{\mathrm{Ro}^{-1}\}f+\zeta\right)=0, \tag{2.1}$$

$$\zeta=\nabla^2\psi, \tag{2.2}$$

$$u=-\frac{\partial\psi}{\partial y}, v=\frac{\partial\psi}{\partial x}. \tag{2.3}$$

where

$$\mathrm{Ro}=\frac{U}{fL}. \tag{2.4}$$

If f is constant, it is the 2D incompressible Euler equation.

2.1 Freely decaying simulation of 2D Euler

We run freely decaying simulation with f constant. We pick the initial energy containing scale of be around 1 and have a 15×15 domain. We use ∇^8 dissipation interpreted spectrally as $k^8+\ell^8$.

Figure 2.1 shows the snap shots of vorticity and the streamfunction over the evolution of the simulation. We see a convincing inverse cascade and the formation of coherent vortices. Figure 2.2 keep track of the kinetic energy and enstrophy. We see that, as expected, they experience a rapid initial decay. Afterwards, they are approximately conserved. Figure 2.3 shows the evolution of the enstrophy spectra. The theoretical expectation is for them to have a k^{-1} slope. We see that this is approximately true in early time. We also see that the hyper-dissipation is damping the small scale effectively.

2.2 Stochastically forced-dissipative simulation

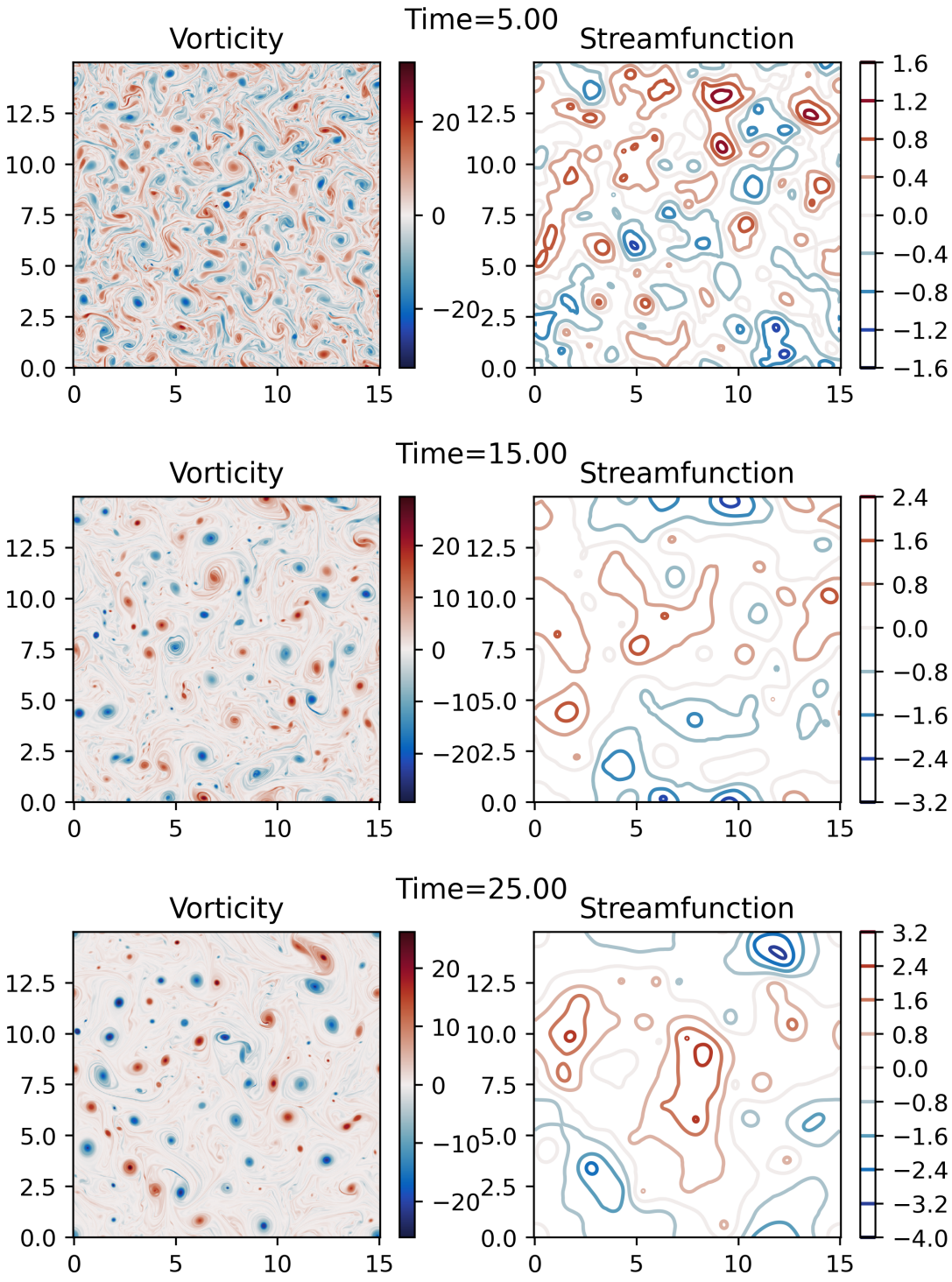

Figure 2.1: Snapshots of vorticity and streamfunction 2D Euler simulation overtime.

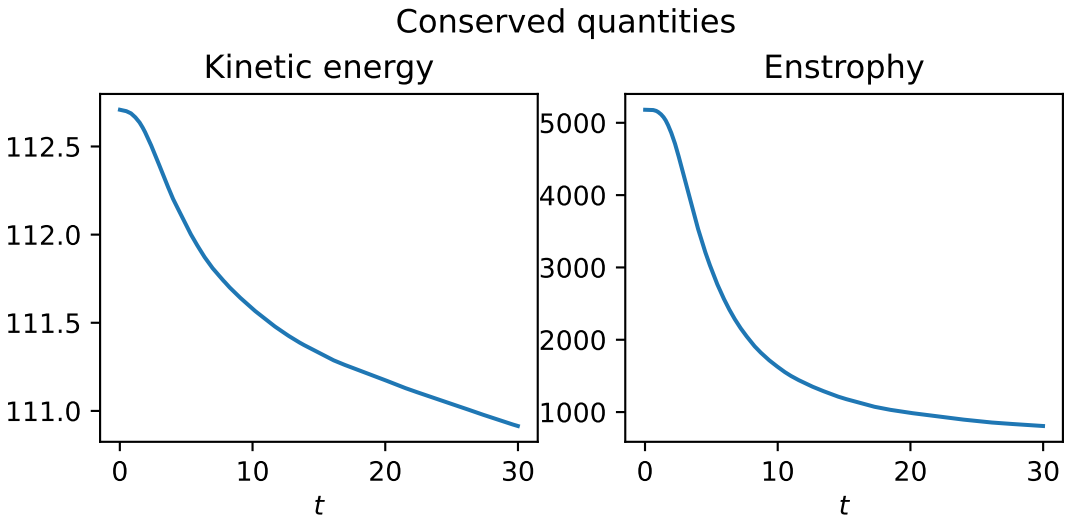

Figure 2.2: Time history of kinetic energy and enstrophy of 2D Euler simulation.

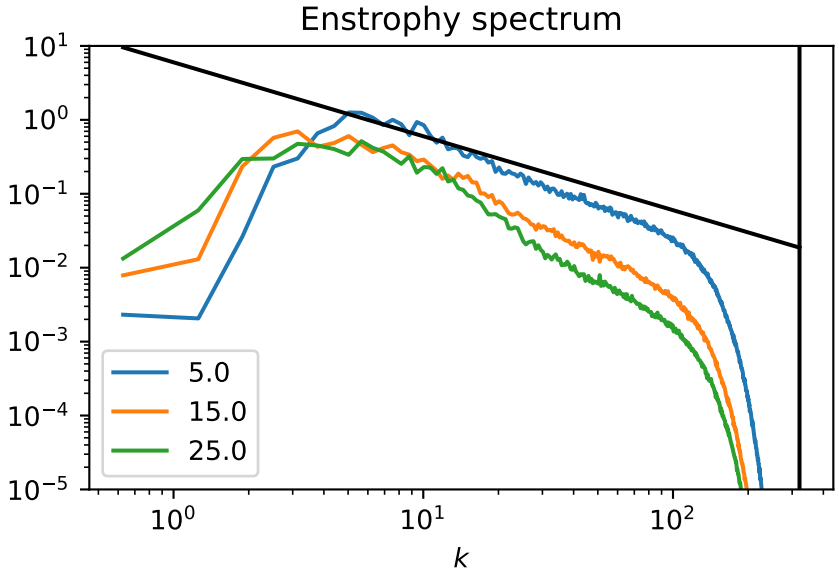

Figure 2.3: Time evolution of the enstrophy spectrum of 2D Euler simulation. Legends shows the time. The slanted black line is the k^{-1} reference and the vertical black line is the maximally resolved wavenumber.

Chapter 3

2D QG-Near Inertial Wave (QG-NIW) model

Ryan Shìjié Dù

The QG-NIW model was derived in Xie and Vanneste 2015. It has been since further explored and expanded by Asselin and Young 2019; Wagner and Young 2015, 2016; Xie 2020 and others. Here we will implement the two-dimensional version in Rocha, Wagner, and Young 2018.

3.1 The QG-NIW model

We have the dimensional QG-NIW model (ignoring dissipation) from ibid., (2.6–8):

$$q = \nabla^2\psi + \frac{1}{f}\left[\frac{1}{4}\nabla^2|\phi|^2 + \frac{i}{2}J(\phi^*,\phi)\right]; \tag{3.1}$$

$$q_t + J(\psi, q) = 0; \tag{3.2}$$

$$\phi_t + J(\psi,\phi) + \phi\frac{i}{2}\nabla^2\psi - \frac{i}{2}\frac{N^2}{fm^2}\nabla^2\phi = 0. \tag{3.3}$$

3.1.1 Nondimensionalization

We make clear the true parameters dependence of the model by nondimensionalizing the model with:

$$\phi \sim U_w = \epsilon^{-1}U_e \tag{3.4}$$

$$\psi \sim U_e L \tag{3.5}$$

$$L \sim L_e = k_e^{-1} \tag{3.6}$$

$$T \sim L/U_e \tag{3.7}$$

where

$$\epsilon = U_e/U_w \ll 1 \tag{3.8}$$

indicated we are in the weak wave regime. Then we get (in the notation of Vallis 1996):

$$q = \nabla^2\psi + \frac{1}{f}\{\alpha\}\left[\frac{1}{4}\nabla^2|\phi|^2 + \frac{i}{2}J(\phi^*,\phi)\right]; \tag{3.9}$$

$$q_t + J(\psi, q) = 0; \tag{3.10}$$

$$\phi_t + J(\psi,\phi) + \phi\frac{i}{2}\nabla^2\psi - \frac{i}{2}\frac{N^2}{fm^2}\{\hbar\}\nabla^2\phi = 0 \tag{3.11}$$

where we have the model depends on only two important nondimensional numbers, the wave amplitude:

$$\alpha = \frac{U_e}{fL}\epsilon^{-2} = \mathrm{Ro}\,\epsilon^{-2}, \tag{3.12}$$

and the wave dispersivity:

$$\hbar = \frac{N^2}{fm^2}\frac{1}{LU_e} = \frac{1}{\mathrm{Ro}}\frac{N^2}{f^2m^2L^2}. \tag{3.13}$$

Note that Rossby number and the small parameter ϵ does not appear explicitly in the model. We only assume that they are small. Instead, their ratio appear as the wave amplitude α. The distinguished limit assumptions in Wagner and Young 2015, 2016; Xie and Vanneste 2015 is $\alpha = 1$. However, in Rocha, Wagner, and Young 2018 it is allowed to vary in the $O(1)$ range. We also noticed that the Rossby number in ibid., Table 4 is wrong. It should be ≈ 0.025. However, the parameters that appear in the equations, $\hbar$ and α, are correct.

The QG-NIW conserves energy and action. In particular we have the two energies (ibid., (3.2)):

$$\mathcal{K} = \frac{1}{2}|\nabla\psi|^2; \tag{3.14}$$

$$\mathcal{P} = \frac{1}{4}\frac{N^2}{f^2m^2}|\nabla\phi|^2. \tag{3.15}$$

After the nondimensionalization, we have the total energy formula

$$\mathcal{P} = \frac{1}{2}|\nabla\psi|^2 + \{\alpha\hbar\}\frac{1}{4}\frac{N^2}{f^2m^2}|\nabla\phi|^2. \tag{3.16}$$

Note the introduction of the nondimensional numbers in from of the potential energy in the formula. They need to be accounted for in order for the total energy formula to be correct.

3.1.2 Separating the real and imaginary fields

In the QG-NIW model, the ϕ field is complex while all other fields are real. If we put the equation as is into Dedalus, all fields must be complex, with the real fields having zero imaginary parts. However, for DFT, real-input require roughly half the computation time of complex-input. This will potentially degrade performance[1]. To address this issue, we write the equation in term of the

[1]See a discussion with the Dedalus developer in https://groups.google.com/u/1/g/dedalus-users/c/habu7iKCCWc/m/mNNGPqLuAwAJ

real and imaginary parts of ϕ. Now all fields can be real. We write the nondimensional equations:

$$q = \nabla^2\psi + \frac{1}{f}\{\alpha\}\left[\frac{1}{4}\nabla^2(\phi_r^2+\phi_i^2)) - J(\phi_r,\phi_i)\right]; \tag{3.17}$$

$$q_t + J(\psi, q) = 0; \tag{3.18}$$

$$\phi_{r,t} + J(\psi,\phi_r) - \frac{\phi_i}{2}\nabla^2\psi + \frac{\hbar}{2}\nabla^2\phi_i = 0 \tag{3.19}$$

$$\phi_{i,t} + J(\psi,\phi_i) + \frac{\phi_r}{2}\nabla^2\psi - \frac{\hbar}{2}\nabla^2\phi_r = 0 \tag{3.20}$$

3.2 2D turbulence modified by NIW

3.2.1 The parameters

We use the set-up of ibid., Tabel 4 & §4.2. We pick the nondimensional parameters

$$\alpha = 0.1 \quad \text{and} \quad \hbar = 1. \tag{3.21}$$

Note that since we have the energy containing scale nondimensionalized to be 1, we have $k_e = 2\pi$ and the domain size to be 10. The k_e value is worth noting when comparing to the results of ibid.

We use the same hyper-diffusivity as ibid., (2.9a, b). We pick $\kappa_e = \nu_w = 8\times10^{-7}$. This is roughly the same dissipation as the numbers in ibid., Tabel 4 as in our nondimensionalization and 512^2 resolution.

3.2.2 The QG-NIW Simulation

We run a 2D Euler simulation to generate the background mean flow using the code in Chapter **??**. We start the energy according to ibid., (4.2) and pick the roughly correct amplitude so that the resulting field matches the amplitude of the ibid. paper.

Then we simulate the QG-NIW model by adding in a wave field of

$$\phi = \frac{1}{\sqrt{2}}(1+i) \tag{3.22}$$

on top of the above PV field. Figure 3.1 shows the result. They compare well with Figure 5 of ibid. We also dianagose the energies and action of the QG-NIW simulation in Figure 3.2. We see convincing conversion of kinetic energy to potential energy and conservation of total energy and wave action.

3.3 Some comments

3.3.1 The IMEX time-stepper and YBJ$^+$ equation

We use the 3rd-order 4-stage DIRK+ERK scheme (`RK443`) for time integration (Ascher, Ruuth, and Spiteri 1997, Sec 2.8). It enjoys the property that the stability region of RK4 includes a

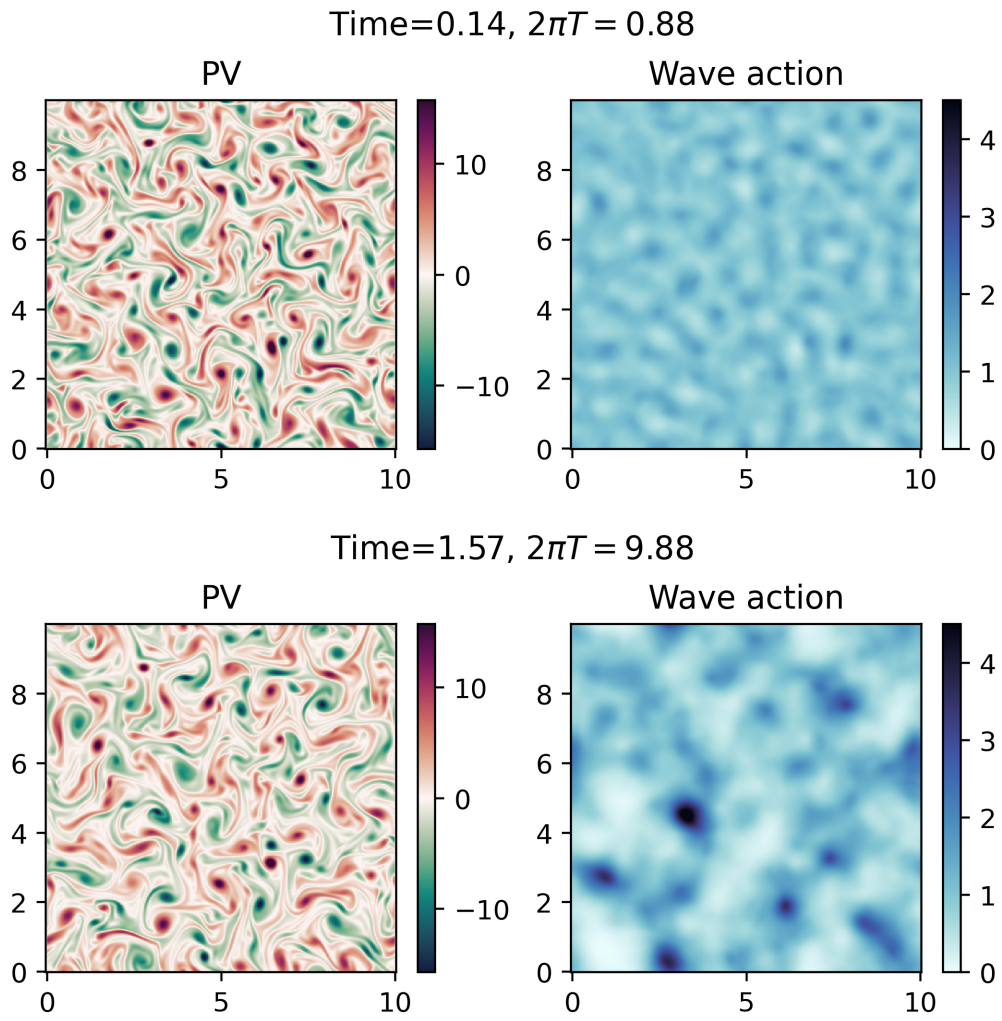

Figure 3.1: Left: the PV field. Right: the Wave action density.

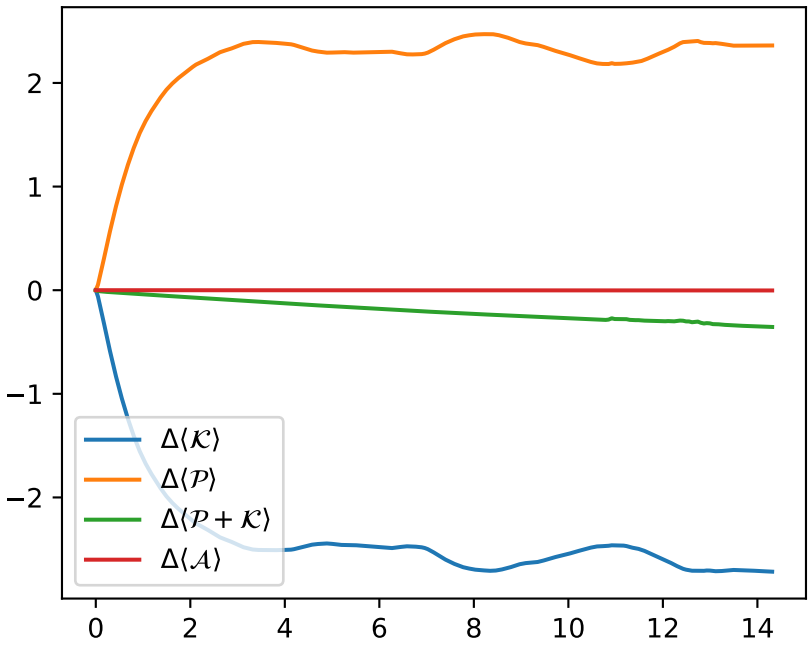

Figure 3.2: The time evolution of energies and action of the QG-NIW model.

portion of the imaginary axis. This is crucial for the stable evolution of the refraction term in the ϕ equation. It is also an implicit-explicit (IMEX) method that treat the stiff linear terms implicitly. This include the dispersion term in (3.11). Therefore we can stably simulate the original QG-NIW system as written in Xie and Vanneste 2015 and Rocha, Wagner, and Young 2018 at high resolution. Asselin and Young 2019 has modified the dispersion term in their YBJ$^+$ equation so that the wave frequency asymptotes to twice the inertial frequency $2f$, instead of growing as k^2. They cite this allows explicit time-stepping of their equations. While this is true, we think this improvement is inconsequential since all turbulence simulation needs small scale dissipation, which is as stiff or stiffer than k^2. We have to treat stiff linear terms implicitly anyway.

However, the IMEX is an imperfect solver for the QG-NIW system. We observe that the action is not monotonically decreasing in our simulation. This might be because the implicit treatment of the dispersion term allows for stable integration, but it does not guarantee conservation of quadratic quantities. Rocha, Wagner, and Young 2018 uses an exponential integrator, which treat the linear terms exactly. It is a more ideal method, but is not yet implemented in Dedalus.

The YBJ$^+$ equation in Asselin and Young 2019 has other benefits of course. To simulate it in Dedalus, we need to be able to define an unusual linear operator, $\mathcal{P}$ in Xie 2020, (3.2). It is currently unclear to us on how to do this. For more see the comments in Section 1.1.3.

With all these caveat, we do not recommend using Dedalus to simulation the QG-NIW system at this time. We recommend a custom implementation using exponential time integrator[2].

[2]A 1D example is `https://github.com/Empyreal092/MMT_Public` (Dù and Bühler 2023).

3.3.2 Another implementation in v2

A Dedalus solver for QG-NIW also exists using Dedalus version 2 (Conn 2023). The current implementation uses the more recent version 3, which is being actively updated. For example, Dedalus only recently (June 25, 2023)[3] allowed restart with partial data in v3 (the `allow_missing` flag in `solver.load_state`). Our version adaptively changes the timestep, therefore is more efficient. Their version uses a lower over RK method, which requires very small timestep for stability, and might suffer the same lack of action conservation.

[3] https://github.com/DedalusProject/dedalus/commit/d3843a7394e06c05bf56ba2710723e42ba19ef39

Chapter 4

Baroclinically unstable two-layer QG

Ryan Shìjié Dù

4.1 The full model nondimensionalized

We start with the 2 layer QG model with mean flow, β, and topography (Vallis 2017, (5.85-86)) (in the notation of Vallis 1996):

$$\frac{\partial q_1}{\partial t} + J(\psi_1, q_1) + U_1 \frac{\partial q_1}{\partial x} + \left(\{\xi_1^{-2}\}\beta + \{\mathrm{Bu}_1^{-1}\} \frac{f_0^2 (U_1 - \{U_r\}U_2)}{g' H_1} \right) \frac{\partial \psi_1}{\partial x} = 0; \tag{4.1}$$

$$\{A\}\frac{\partial q_2}{\partial t} + J(\psi_2, q_2) + U_2 \frac{\partial q_2}{\partial x} + \left(\{\xi_2^{-2}\}\beta + \{\mathrm{Bu}_2^{-1}\} \frac{f_0^2 (U_2 - \{U_r^{-1}\}U_1)}{g' H_2} \right) \frac{\partial \psi_2}{\partial x} = 0. \tag{4.2}$$

where

$$q_1 = \nabla^2 \psi_1 + \{\mathrm{Bu}_1^{-1}\} \frac{f_0^2}{g' H_1} (\{U_r\}\psi_2 - \psi_1); \tag{4.3}$$

$$q_2 = \nabla^2 \psi_2 + \{\mathrm{Bu}_2^{-1}\} \frac{f_0^2}{g' H_2} (\{U_r^{-1}\}\psi_1 - \psi_2) + \left\{ \frac{\alpha}{\mathrm{Ro}_2} \right\} \frac{f_0}{H_2} \eta. \tag{4.4}$$

We have nondimensionalized time to be the advective timescale of the first layer:

$$T = \frac{L_1}{U_1}. \tag{4.5}$$

Then we nondimensionalized (4.1) and (4.3) with length L_1 and (4.2) and (4.4) with length L_2. We have introduced the nondimensional number ξ which is the ratio between the Rhine scale and the lengthscale of each layer (Held and Larichev 1996)

$$\xi_i^{-2} = \frac{\beta L_i^2}{|U_i|} \tag{4.6}$$

and α which is the ratio of the typical topographic height versus the second layer's height

$$\alpha = \frac{\eta}{H_2}. \tag{4.7}$$

If the height and mean flow of the two layers are not equal, we have two parameters for their ratio

$$U_r = \frac{|U_2|}{|U_1|}, \quad \text{and} \quad A = \frac{|U_1|L_2}{|U_2|L_1} \tag{4.8}$$

We also have the more familiar quantities

$$L_{i,d} = \frac{\sqrt{g'H_i}}{f_0} \quad , \quad \mathrm{Ro}_2 = \frac{|U_2|}{f_0 L_2} \quad \text{and} \quad \mathrm{Bu}_i = \frac{L_{i,d}^2}{L_i^2}. \tag{4.9}$$

4.2 The symmetric, flat bottom case

4.2.1 The simplified model

The equation simplifies drastically when we make the upper/lower layer symmetry assumption (Larichev and Held 1995). We take $H_1 = H_2 = H/2$ and $U_1 = -U_2 = U$. Then the equation becomes

$$\frac{\partial q_1}{\partial t} + J(\psi_1, q_1) + U\frac{\partial q_1}{\partial x} + \left(\{\xi^{-2}\}\beta + \{8\mathrm{Bu}^{-1}\}\frac{4f_0^2 U}{g'H}\right)\frac{\partial \psi_1}{\partial x} = 0, \tag{4.10}$$

$$\frac{\partial q_2}{\partial t} + J(\psi_2, q_2) - U\frac{\partial q_2}{\partial x} + \left(\{\xi^{-2}\}\beta - \{8\mathrm{Bu}^{-1}\}\frac{4f_0^2 U}{g'H}\right)\frac{\partial \psi_2}{\partial x} = 0; \tag{4.11}$$

where

$$q_1 = \nabla^2\psi_1 + \{4\mathrm{Bu}^{-1}\}\frac{2f_0^2}{g'H}(\psi_2 - \psi_1), \tag{4.12}$$

$$q_2 = \nabla^2\psi_2 + \{4\mathrm{Bu}^{-1}\}\frac{2f_0^2}{g'H}(\psi_1 - \psi_2) + \left\{\frac{\alpha}{\mathrm{Ro}}\right\}\frac{2f_0}{H}\eta. \tag{4.13}$$

We have

$$\xi^{-2} = \frac{\beta L^2}{U} \quad , \quad \mathrm{Bu} = \frac{2g'H}{f_0^2 L^2} = \frac{L_d^2}{L^2} \quad \text{and} \quad \alpha = \frac{2\eta}{H}. \tag{4.14}$$

Note that this implies (cf. Vallis 2017, (9.103))

$$L_d = \frac{2\sqrt{g'H/2}}{f_0} \quad \text{with} \quad k_d^2 = \frac{4f_0^2}{g'H} = \frac{8}{L_d^2}. \tag{4.15}$$

This is an ok definition when we connect to the continuously stratified case by using (cf. ibid., (5.138))

$$L_d = \frac{NH}{f} \quad \text{with} \quad N^2 = \frac{g'}{H/2}. \tag{4.16}$$

ξ and Bu are not independent since their only freedom is in picking L. In our simulation, we pick $L = L_d$ such that $\mathrm{Bu} = 1$. We further simplify by setting flat topography ($\alpha = 0$). The only free parameter is ξ

$$\xi^{-2} = \frac{\beta L^2}{U} = \frac{\beta L_d^2}{U} \tag{4.17}$$

It is the two-layer version of the 'Charney–Green number'.

4.2.2 Linear stability analysis

We take only the linear terms of the above model, and dispense of all unnecessary parameters:

$$\frac{\partial q_1}{\partial t} + \frac{\partial q_1}{\partial x} + \left(\xi^{-2} + 8\mathrm{Bu}^{-1}\right)\frac{\partial \psi_1}{\partial x} = 0, \tag{4.18}$$

$$\frac{\partial q_2}{\partial t} - \frac{\partial q_2}{\partial x} + \left(\xi^{-2} - 8\mathrm{Bu}^{-1}\right)\frac{\partial \psi_2}{\partial x} = 0; \tag{4.19}$$

where

$$q_1 = \nabla^2\psi_1 + 4\mathrm{Bu}^{-1}(\psi_2 - \psi_1), \tag{4.20}$$

$$q_2 = \nabla^2\psi_2 + 4\mathrm{Bu}^{-1}(\psi_1 - \psi_2). \tag{4.21}$$

This system if isomorphic to ibid., (9.107). Therefore we can copy down the answer:

$$c = -\frac{\xi^{-2}}{K^2 + 8\mathrm{Bu}^{-1}}\left\{1 + \frac{8\mathrm{Bu}^{-1}}{2K^2} \pm \frac{8\mathrm{Bu}^{-1}}{2K^2}\left[1 + 4\frac{K^4(K^4 - 8^2\mathrm{Bu}^{-2})}{8^2\xi^{-4}\mathrm{Bu}^{-2}}\right]^{1/2}\right\}. \tag{4.22}$$

We have recovered ibid., (9.114) with $\hat{k}_d^2 = 8$ and (cf. ibid., (9.115))

$$\xi^{-2} = \hat{k}_\beta^2 = \frac{\beta L_d^2}{U}. \tag{4.23}$$

If we pick $\xi = 2$ following Held and Larichev 1996, Table 1, this means that

$$\frac{\hat{k}_\beta}{\hat{k}_d} = \frac{1}{4\sqrt{2}} \tag{4.24}$$

which quantifies the amount of inverse cascade between the energy injection scale of baroclinic instability and the arrest by β.

Bibliography

Ascher, Uri M., Steven J. Ruuth, and Raymond J. Spiteri (Nov. 1, 1997). "Implicit-Explicit Runge-Kutta Methods for Time-Dependent Partial Differential Equations". In: *Applied Numerical Mathematics*. Special Issue on Time Integration 25.2, pp. 151–167. ISSN: 0168-9274. DOI: 10.1016/S0168-9274(97)00056-1.

Asselin, Olivier and William R. Young (Oct. 2019). "An Improved Model of Near-Inertial Wave Dynamics". In: *Journal of Fluid Mechanics* 876, pp. 428–448. ISSN: 0022-1120, 1469-7645. DOI: 10.1017/jfm.2019.557.

Callies, Jörn et al. (Feb. 10, 2016). "The Role of Mixed-Layer Instabilities in Submesoscale Turbulence". In: *Journal of Fluid Mechanics* 788, pp. 5–41. ISSN: 0022-1120, 1469-7645. DOI: 10.1017/jfm.2015.700.

Conn, Scott (2023). *2DYBJ-QG*. URL: https://github.com/scott-conn/2DYBJ-QG.

Dù, Ryan Shìjié and Oliver Bühler (July 14, 2023). "The Impact of Frequency Bandwidth on a One-Dimensional Model for Dispersive Wave Turbulence". In: *Journal of Nonlinear Science* 33.5, p. 81. ISSN: 1432-1467. DOI: 10.1007/s00332-023-09936-8.

Eady, E. T. (1949). "Long Waves and Cyclone Waves". In: *Tellus* 1.3 (3), pp. 33–52. ISSN: 2153-3490. DOI: 10.1111/j.2153-3490.1949.tb01265.x.

Held, Isaac M. and Vitaly D. Larichev (Apr. 1, 1996). "A Scaling Theory for Horizontally Homogeneous, Baroclinically Unstable Flow on a Beta Plane". In: *Journal of the Atmospheric Sciences* 53.7 (7), pp. 946–963. ISSN: 00224928. DOI: 10.1175/1520-0469(1996)053<0946:ASTFHH>2.0.CO;2.

Larichev, Vitaly D. and Isaac M. Held (Oct. 1, 1995). "Eddy Amplitudes and Fluxes in a Homogeneous Model of Fully Developed Baroclinic Instability". In: *Journal of Physical Oceanography* 25.10, pp. 2285–2297. ISSN: 0022-3670, 1520-0485. DOI: 10.1175/1520-0485(1995)025<2285:EAAFIA>2.0.CO;2.

Majda, A J, D W Mclaughlin, and E G Tabak (1997). "A One-Dimensional Model for Dispersive Wave Turbulence". In: *J. Nonlinear Sci* 6, pp. 9–44. DOI: 10.1007/BF02679124.

Pierrehumbert, Raymond T., Isaac M. Held, and Kyle L. Swanson (June 1, 1994). "Spectra of Local and Nonlocal Two-Dimensional Turbulence". In: *Chaos, Solitons & Fractals*. Special Issue: Chaos Applied to Fluid Mixing 4.6, pp. 1111–1116. ISSN: 0960-0779. DOI: 10.1016/0960-0779(94)90140-6.

Rocha, Cesar B., Gregory L. Wagner, and William R. Young (July 2018). "Stimulated Generation: Extraction of Energy from Balanced Flow by near-Inertial Waves". In: *Journal of Fluid Mechanics* 847, pp. 417–451. ISSN: 0022-1120, 1469-7645. DOI: 10.1017/jfm.2018.308.

Smith, K. S. et al. (Oct. 2002). "Turbulent Diffusion in the Geostrophic Inverse Cascade". In: *Journal of Fluid Mechanics* 469, pp. 13–48. ISSN: 1469-7645, 0022-1120. DOI: 10.1017/S0022112002001763.

Tulloch, Ross and K. Shafer Smith (Apr. 1, 2009). "A Note on the Numerical Representation of Surface Dynamics in Quasigeostrophic Turbulence: Application to the Nonlinear Eady Model".

In: *Journal of the Atmospheric Sciences* 66.4, pp. 1063–1068. ISSN: 0022-4928, 1520-0469. DOI: 10.1175/2008JAS2921.1.

Vallgren, Andreas and Erik Lindborg (2011). "The Enstrophy Cascade in Forced Two-Dimensional Turbulence". In: *Journal of Fluid Mechanics* 671, pp. 168–183. ISSN: 00221120. DOI: 10.1017/S0022112010005562.

Vallis, Geoffrey K. (1996). "Potential Vorticity Inversion and Balanced Equations of Motion for Rotating and Stratified Flows". In: *Quarterly Journal of the Royal Meteorological Society* 122.529, pp. 291–322. ISSN: 1477-870X. DOI: 10.1002/qj.49712252912.

— (Aug. 2016). "Geophysical Fluid Dynamics: Whence, Whither and Why?" In: *Proceedings of the Royal Society A: Mathematical, Physical and Engineering Sciences* 472.2192, p. 20160140. DOI: 10.1098/rspa.2016.0140.

— (2017). *Atmospheric and Oceanic Fluid Dynamics: Fundamentals and Large-Scale Circulation*. 2nd ed. Cambridge: Cambridge University Press. ISBN: 978-1-107-06550-5. DOI: 10.1017/9781107588417.

Wagner, Gregory L. and William R. Young (Dec. 2015). "Available Potential Vorticity and Wave-Averaged Quasi-Geostrophic Flow". In: *Journal of Fluid Mechanics* 785, pp. 401–424. ISSN: 0022-1120, 1469-7645. DOI: 10.1017/jfm.2015.626.

— (Sept. 2016). "A Three-Component Model for the Coupled Evolution of near-Inertial Waves, Quasi-Geostrophic Flow and the near-Inertial Second Harmonic". In: *Journal of Fluid Mechanics* 802, pp. 806–837. ISSN: 0022-1120, 1469-7645. DOI: 10.1017/jfm.2016.487.

Xie, Jin-Han (Dec. 2020). "Downscale Transfer of Quasigeostrophic Energy Catalyzed by Near-Inertial Waves". In: *Journal of Fluid Mechanics* 904, A40. ISSN: 0022-1120, 1469-7645. DOI: 10.1017/jfm.2020.709.

Xie, Jin-Han and J. Vanneste (July 10, 2015). "A Generalised-Lagrangian-mean Model of the Interactions between near-Inertial Waves and Mean Flow". In: *Journal of Fluid Mechanics* 774, pp. 143–169. ISSN: 0022-1120, 1469-7645. DOI: 10.1017/jfm.2015.251.